On the use of mode shape curvatures for damage localization under varying environmental conditions

Received: 28 December 2016 | Revised: 8 September 2017 | Accepted: 22 November 2017

DOI: 10.1002/stc.2132

RESEARCH ARTICLE

WILEY

On the use of mode shape curvatures for damage localization under varying environmental conditions

Yaser Shokrani[1] | Vasilis K. Dertimanis[2] | Eleni N. Chatzi[2] | Marco N. Savoia[1]

[1]Department of Civil, Chemical, Environmental, and Materials Engineering, University of Bologna, 40126 Bologna, Italy

[2]Department of Civil, Environmental and Geomatic Engineering, Institute of Structural Engineering, 8093 ETH Zürich, Switzerland

Correspondence
Eleni N. Chatzi, Chair of Structural Mechanics, Institute of Structural Engineering, Department of Civil, Environmental and Geomatic Engineering, 8093 ETH Zürich, Switzerland.
Email: chatzi@ibk.baug.ethz.ch

Funding information
Albert Lück foundation

Summary

A novel damage localization method is introduced in this study, which exploits mode shape curvatures as damage features, while accounting for operational variability. The developed framework operates in an output-only regime,that is, it does not assume availability of records from the influencing environmental/operational quantities but rather from response quantities alone. The introduced tool comprises 3 stages pertaining to training, validation, and diagnostics. During the training stage, a representation of the healthy, or baseline, structural state is acquired over varying operational conditions. A data matrix is formulated, whose individual columns correspond to mode shape curvatures at distinct operational conditions, and principal component analysis (PCA) is applied for extraction of the imprints of separate operational sources on these curvatures. To this end, a residual matrix between the original and the PCA mapped data is formed serving for statistical characterization of each mode. Subsequently, during the validation and diagnostics stages, the mode shape curvature matrices for the currently inspected structural state are assembled and the same PCA mapping is enforced. A typical hypothesis test and a corresponding damage index are then adopted in order to firstly detect damage, and to secondly localize damage, should this exist. The implementation of the proposed method in 2 numerical case studies confirms its effectiveness and the encouraging results suggest further investigation on operating structural systems.

KEYWORDS

damage detection and localization, environmental and operational variability, mode shape curvature, principal component analysis, structural health monitoring

1 | INTRODUCTION

Civil and mechanical structures are continually advancing in form and complexity but are inevitably exposed to damage and deterioration since the very first day of operation. At this point in time, developed societies are faced with the issue of managing and maintaining the significant portion of existing infrastructure, which has reached the end of its design lifespan. In an effort to handle this issue in a sustainable manner, the concept of structural health monitoring (SHM)

has emerged in the last decades.[1] SHM relies on monitoring-based supervision, which is commonly carried out in a continuous and long-term manner, as opposed to the traditional practice of visual inspection, which is inevitably periodic and often biased to expert judgment.[2] Over the past 35 years, SHM has been the focus of widespread growing attention of both scholars and practitioners and has evolved rapidly as a result of its economic and safety benefits.[3]

In its broad definition, structural health monitoring pertains to the set of methods and tools concerned with the tracking of structural condition with the purpose of ensuring safety, integrity, and optimal operation and maintenance of infrastructure.[4-6] SHM comprises four distinct levels,[7] namely, (a) detection of the presence of damage; (b) localization of induced damage; (c) quantification of the severity and extent of damage; and (d) estimation of the remaining service life of the structure. As damage alarms and intervention triggers are often considered the more critical and urgent tasks, the former two categories have attracted the largest share of attention in existing literature. The damage detection procedure typically decomposes sensory information into features that are indicative of the structure's condition, also referred to as "health." In this context, damage is often defined as a deviation, in the statistical sense, of the damaged system features when compared against their baseline, or healthy, signatures.

In picking up such discrepancies, vibration-based methods are often adopted, which rely on the system's dynamic properties for discriminating between a healthy and unsound structure.[8] The underlying idea in these methods is that a change in the vibration properties, such as modal frequency, modal shape, or mode shape curvature (MSC),[9] is a signal of induced damage in the structure.[10, 11] A very comprehensive literature review of these methods is available in the works of Doebling et al.,[12] Sohn et al.,[13] and Limongelli et al.,[14] whereas further explorations can be found in Catbas et al.,[15] Catbas and Aktan,[16] and Aktan et al.[17] It should be noted that the behavior of engineered systems does not always comply with the commonly adopted simplifications of multiple degrees of freedom (DOFs) and vibration modes. However, for some systems in particular, these simplifications do hold to a great extent. This includes systems that are broadly exploited in the context of civil infrastructure, such as girder bridges and shear frames. A number of works in fact prove efficacy of damage detection schemes on such systems. In this context, George et al.[18] employ a measure relying on normalized energies derived from accelerometers that are distributed on railway bridge structures, demonstrating a direct link between damage localization and the spatial arrangement of the sensing system. On the other hand, for the case of shear-type frame structures, Celebi et al.[19] employ interstory drift ratios to estimate damage, once again exploiting the equivalence of the system to a simplified model.

In a significant portion of published studies on this topic, the environmental factors and their effect on variation of vibration characteristics of the structure are neglected for the sake of simplicity, with environmental conditions are assumed to be constant. However, in practice, the structure is subject to continually changing environments, for example, temperature and humidity conditions, throughout its life cycle often masking the changes induced by actual damage or deterioration.[20-22] The notable influence of varying environmental and operational effects, for example, traffic loads, is noted in the works of Farrar et al.,[23] Alampalli,[24] Peeters and De Roeck,[25] and Cross et al.,[26] where changes of the order of up to 50% are observed on natural frequencies. This practical challenge has been addressed more recently in a number of works,[27-30] attempting to link environmental influences to the evolution of structural parameters, in an effort to reduce the uncertainty in the monitoring and diagnostics procedures.

The driving principle behind the aforementioned studies lies in simulation of the influence of environmental variation onto modal parameters and subsequent separation of this from additional variations, which could be a consequence of damage or irregularity.[31-34] In this context, it is necessary to derive a baseline model for the healthy (or reference) structural state in order to further recognize irregularities that may be attributed to damage.[35-37] In this sense, Dervilis et al.[38] present a robust regression framework for linking measured input quantities, such as temperature and wind speed, to output response data, such as monitored natural frequencies of the Z24 and Tamar bridge. Spiridonakos and Chatzi[39] employ a Polynomial Chaos Expansion on the Z24 bridge benchmark for furnishing a functional relationship between input and output quantities, by exploiting available knowledge on the probabilistic distributions of the input. To the same end, Peeters and De Roeck employ ARX-type models,[25] whereas Magãlhaes et al.[40] adopt dynamic regression models of the variations of natural frequencies with respect to deck temperatures, deck vibration amplitudes, and modal damping, to indirectly quantify the influence of the traffic jams over the bridge deck on the natural frequencies. However, a major drawback of techniques relying on regression lies in the assumption of availability of environmental or operational load records, often in multiple locations across the structure. Consequently, the optimized number and positioning of sensors that prove adequate in capturing both the environmental influence and potential damage effects comprise a challenge.[41, 42] An obvious obstacle lies in the lack of access to direct measurements of operational influences such as traffic, wind loads, or distributed temperature gradients, which may often result in neglecting sources of considerable impact.

In alleviating the need for a direct measurement of environmental or operational variations, a number of output-only methodologies have been developed, which treat these quantities as embedded variables. Bernal[43] provides an interesting overview of the damage detection and localization problem in civil engineering structures when environmental metrics are not directly measured. In this context, Figueiredo et al.[44] employ machine learning alternatives; Harmanci et al. [45] adopt output-only autoregressive models; Sohn et al.[46] and Dervilis et al.[47] rely on auto-associative neural networks; whereas Lämsä & Kullaa[42, 48] exploit factor analysis. A notable class of works in this domain takes advantage of principle component analysis (PCA) as a means of accounting for the effect of environmental and operational factors.[49] PCA[50] seeks to convert a set of correlated data into a set of linearly uncorrelated ones, deemed *principal components*. This is achieved via a linear transformation aiming at reducing dimensionality while retaining the salient information contained in the data. PCA is thus capable of revealing hidden patterns underlying complex data sets,[51] thereby finding application across diverse fields including signal processing (e.g., the discrete Kosambi-Karhunen-Loève transform), mechanical engineering and rotating machinery (e.g., the singular spectrum analysis and the proper orthogonal decomposition), and mathematics (e.g., the singular value decomposition). The interested reader is referred to Jolliffe[52] for a thorough review. Applications in structural engineering include modal analysis,[53] model updating,[54] reduced order modeling,[55] and damage identification.[56, 57]

Within this context, Yan et al. successfully detect the presence of damage in both an experimental and simulated data in varying environmental conditions by performing PCA on modal frequencies as features.[58, 59] Reynders et al.[60] introduce an improved technique based on kernel principal component analysis. Nguyen et al.[61] suggest a time domain approach to PCA for identifying damage on a bridge in Luxemburg, as well as a frequency domain approach to PCA, which exploits availability of mode shapes and of an estimated frequency response function, for localization of damage. Hoell and Omenzetter[62] perform damage detection by applying PCA on the partial autocorrelation coefficients of acceleration response records obtained in the healthy and damaged states. In an attempt to perform damage classification, Tibaduiza et al.[63] combine PCA and self-organizing maps. Li et al.[64] propose the use of a modal sensitivity matrix as a damage-sensitive feature for use with PCA (see also Koo et al.[65]), whereas Li et al.[66] study the effects of wind and temperature on the modal frequencies, mode shapes, and damping ratios. Jin et al.[67] propose an adaptive scheme for updating the reference information when performing damage detection under varying environmental conditions, and Bellino et al. present a PCA-based approach to detect damage in time-varying systems.[68]

The majority of the previous studies focuses on the first level of the SHM process, that is, detection and possibly classification. The current paper proceeds one step further, presenting a PCA-based approach to damage localization and classification under varying environmental conditions. To this end, the MSCs are adopted in this work as features that enable higher level SHM procedures. To the best of the knowledge of the authors, the MSCs[69-71] have never been used thus far as a vibration feature in conjunction with the PCA. The aim of this study is to fill this gap and explore this issue by proposing a simple, straightforward, and effective framework for damage localization under changing operational conditions. To this end, a structural system that is amenable to environmental/operational changes over a long-term horizon is considered. Given a number of monitored vibration modes, the MSCs are defined as the directional derivatives of the mode shapes along a specific direction. Under normal operating conditions, the variation of the calculated MSCs is tied to the independent sources of operational variability.

Accordingly, PCA is applied to the MSCs in a process that comprises a training, validation, and diagnostic stage: In the first, the MSC data matrices are formulated across a representative operational period, a residual matrix is calculated, and the statistical characterization of each node is estimated. In the validation and diagnostic stages, the corresponding MSC data matrices are decomposed using the PCA mapping established during the training stage. A simple hypothesis test and an induced damage index are then utilized for achieving damage detection and localization, with the latter depending on the type of considered vibration modes. The developed approach is exemplified through two simulated applications, across different scenarios of environmental variation, with results validating efficiency and robustness.

2 | A FRAMEWORK FOR DAMAGE LOCALIZATION

2.1 | Problem statement

Consider a structural system $S(\tau, t)$ with n DOFs, which may be represented by a second-order vector differential equation of the form

$$\mathbf{M}(\tau)\ddot{\mathbf{x}}(t) + \mathbf{C}(\tau)\dot{\mathbf{x}}(t) + \mathbf{K}(\tau)\mathbf{x}(t) = \mathbf{P}(\tau)\mathbf{f}(t), \tag{1}$$

where $\mathbf{x}(t)$ corresponds to the $[n \times 1]$ vector of dynamic displacements; $\mathbf{M}(\tau)$, $\mathbf{C}(\tau)$, and $\mathbf{K}(\tau)$ are the $[n \times n]$ mass, viscous damping, and stiffness matrices, respectively; and $\mathbf{f}(t)$ is the $[m \times 1]$ excitation vector, acting on the structure as defined by the $[n \times m]$ allocation matrix $\mathbf{P}(\tau)$.

The above form of Equation 1 implies that $\mathcal{S}(\tau, t)$ responds on two time scales: The *short-term scale*, expressed by the temporal quantity t, pertains to structural response due to the effects of the excitation $\mathbf{f}(t)$, whereas the *long-term scale*, expressed by the temporal quantity τ, pertains to variation of structural properties due to slowly evolving phenomena, such as the interaction of the structure with its environment. Although no explicit unit need be assigned to the long-term scale, it is herein assumed that it can be clearly distinguished from the short scale, thus rendering the structure described by Equation 1 a (slowly) time-varying system.

The vibration modes of $\mathcal{S}(\tau, t)$ are characterized by the set

$$\mathcal{M}(\tau) = \left\{ \omega_j(\tau), \zeta_j(\tau), \Phi_j(\tau) | \, j = 1, \, \dots \, , n \right\}, \tag{2}$$

where $\omega_j(\tau)$, $\zeta_j(\tau)$, and $\mathbf{\Phi}_j(\tau)$ correspond to the natural frequencies, the damping ratios, and the mode shapes, respectively, of the jth mode. Without loss of generality, it is assumed that vectors $\mathbf{\Phi}_j(\tau)$ correspond to the normal modes of the structure. It should be noted that the analysis that follows can be further generalized to structures characterized by complex mode shapes. Equation 2 implies that under normal operating conditions, that is, without structural damage, the vibration modes will vary only with respect to effects evolving in the long-term scale.

At this point, we shift from the notion of DOFs of dimension n, to the finite number of nodes p in which a system is commonly discretized and monitored, with each node aggregating information over multiple directions and corresponding DOFs, as illustrated in Figure 1. In this context, the mode shapes may be broken down into their components along the individual main axes x, y, z:

$$\Phi_j(\tau) = \left[\Phi_{j,x}^T(\tau) \Phi_{j,y}^T(\tau) \Phi_{j,z}^T(\tau) \right]^T, \; j = 1, \, \dots \, , n. \tag{3}$$

The MSC for each mode j and along each distinct direction x, y, or z may then be recovered by the well-known central difference approximation formula at all available grid points $k = 1, \, \dots \, , p$:

$$\Psi_{j,x}(\tau, k) = \frac{\Phi_{j,x}(\tau, k+1) - 2\Phi_{j,x}(\tau, k) + \Phi_{j,x}(\tau, k-1)}{\Delta x^2} \tag{4a}$$

$$\Psi_{j,y}(\tau, k) = \frac{\Phi_{j,y}(\tau, k+1) - 2\Phi_{j,y}(\tau, k) + \Phi_{j,y}(\tau, k-1)}{\Delta y^2} \tag{4b}$$

$$\Psi_{j,z}(\tau, k) = \frac{\Phi_{j,z}(\tau, k+1) - 2\Phi_{j,z}(\tau, k) + \Phi_{j,z}(\tau, k-1)}{\Delta z^2}, \tag{4c}$$

for $j = 1, \, \dots \, , n$, where $k \pm 1$ indicates the neighboring node along the given direction. As explained in what follows, damage detection and localization is herein achieved via efficient simulation of the long-term evolution of the MSC quantities defined in Equation 4.

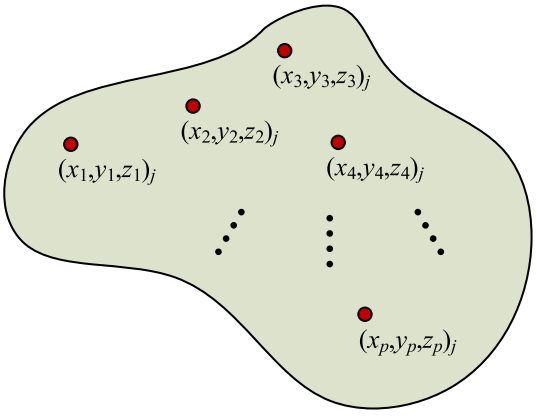

FIGURE 1 Mapping of the jth normal mode shape to the nodes of $S(\tau, t)$

2.2 | Principal component analysis

Assume that MSC data is available at distinct long-term time instants $\tau_1, \tau_2, \ldots, \tau_q$. Then for each directional derivative of Equation 4, the following $[p \times q]$ matrix can be formulated for every vibration mode, where subscripts j and x, y, z are henceforth omitted

$$\mathbf{D} = \begin{bmatrix} \Psi(\tau_1, 1) & \Psi(\tau_2, 1) & \ldots & \Psi(\tau_q, 1) \\ \Psi(\tau_1, 2) & \Psi(\tau_2, 2) & \ldots & \Psi(\tau_q, 2) \\ \vdots & \vdots & \ddots & \vdots \\ \Psi(\tau_1, p) & \Psi(\tau_2, p) & \ldots & \Psi(\tau_q, p) \end{bmatrix}. \tag{5}$$

By applying the PCA, $\mathbf{D}$ can be linearly mapped to a matrix $\mathbf{K}$ of lower dimension

$$\mathbf{K} = \mathbf{T}\mathbf{D}, \tag{6}$$

where $\mathbf{K} \in \mathbb{R}^{d \times q}$ and $\mathbf{T} \in \mathbb{R}^{d \times p}$ are referred to as the *scores* and *loading* matrices, respectively. Both the required dimension d and matrix $\mathbf{T}$ are calculated through the singular value decomposition of the covariance matrix of $\mathbf{D}$

$$\frac{1}{q}\mathbf{D}\mathbf{D}^T = \mathbf{U}\Sigma^2\mathbf{U}^T, \tag{7}$$

where $\mathbf{U} \in \mathbb{R}^{p \times p}$ is orthogonal, whereas $\Sigma \in \mathbb{R}^{p \times p}$ is diagonal and contains the singular values. The latter can be grouped in two subsets by rewriting the right hand side of Equation 7 as

$$\begin{bmatrix} \mathbf{U}_1 & \mathbf{U}_2 \end{bmatrix} \begin{bmatrix} \Sigma_1 & \mathbf{O} \\ \mathbf{O} & \Sigma_2 \end{bmatrix} \begin{bmatrix} \mathbf{U}_1^T \\ \mathbf{U}_2^T \end{bmatrix}, \tag{8}$$

with

$$\Sigma_1 = \mathrm{diag}\{\sigma_1, \sigma_2, \ldots, \sigma_d\} \tag{9a}$$

$$\Sigma_2 = \mathrm{diag}\{\sigma_{d+1}, \sigma_{d+2}, \ldots, \sigma_q\} \tag{9b}$$

and

$$\sigma_1 \geq \sigma_2 \geq \ldots \geq \sigma_d > 0 \approx \sigma_{d+1} = \cdots = \sigma_q \tag{10}$$

implying that the trailing subset of singular values is negligible and can be discarded. From Equations (7)–(10), it follows that

$$\frac{1}{q}\mathbf{D}\mathbf{D}^T \approx \mathbf{U}_1\Sigma_1^2\mathbf{U}_1^T, \tag{11}$$

where for $\mathbf{U}_1 \in \mathbb{R}^{p \times d}$, orthogonality is maintained. One can thus select $\mathbf{T} = \mathbf{U}_1^T$.

The dimension $d \ll p$ corresponds herein to the number of all individual sources (e.g., environmental factors and traffic loads) that affect the MSC under normal operating conditions in the long-term scale. It must be emphasized that any individual source of structural uncertainty is reflected in d, as long as it is systematic. In general, the choice of an appropriate value for d is not critical and, usually, a range of values may lead to similar results in terms of reliability, accuracy, and consistency. It should however be noted that the selection of either quite low or very high values of d may result in an inadequate mapping. In the former case, the selection discards the (possibly) many influencing factors and renders the method unable to represent the inherent variation, whereas in the latter case, the probability of overfitting is increased.

2.3 | Damage detection and localization

Following the previous formulation, Figure 2 illustrates the proposed damage detection and localization strategy. The procedure initiates with the training stage in the healthy, or baseline, structural state, during which a *representative* population of temporal points in the long-term scale and a number of characteristic vibration modes are selected (input parameters τ_q and n, respectively). The term representative implies that the training set should reflect a range of variations of the influencing agents. The set of temporal points, $\mathcal{T}(\tau) = \{\tau_1, \tau_2, \ldots, \tau_q\}$, is then split into two subsets, the estimation $\mathcal{T}_e(\tau)$ and validation $\mathcal{T}_v(\tau)$ set, with $\mathcal{T}_e(\tau) \cup \mathcal{T}_v(\tau) = \mathcal{T}(\tau)$ and $\mathcal{T}_e(\tau) \cap \mathcal{T}_v(\tau) = \emptyset$. For each of the temporal points included in $\mathcal{T}_e(\tau)$, the matrices $\mathbf{D}_j$ are formulated for $j = 1, 2, \ldots, n$. Accordingly, PCA as described in the previous section is applied, and the dimension d and the loading matrices $\mathbf{T}_j$ are estimated. A PCA-based approximation of the original data matrix appearing in Equation 5 for mode j, $\widehat{\mathbf{D}}_j$ may be obtained by re-mapping the projected data back to the original space as

$$\hat{\mathbf{D}}_j = \mathbf{T}_j^T \mathbf{K}_j = \mathbf{T}_j^T \mathbf{T}_j \mathbf{D}_j, \quad j = 1, 2, \ldots, n. \tag{12}$$

The loss of information from this mapping can be assessed by a residual matrix $\mathbf{R}_j$ as

$$\mathbf{R}_j = \mathbf{D}_j - \hat{\mathbf{D}}_j, \tag{13}$$

the kth individual row of which, herein notated as $[\mathbf{R}_j]_{k,*}$, quantifies the loss of information at every node of the structure, from the mapping and recovery process. A statistical distribution is then fitted to the samples of every $[\mathbf{R}_j]_{k,*}$ vector. It will be henceforth assumed that each of the row samples of the $\mathbf{R}_j$ matrices can be approximated by a normal distribution. This is by no means a restrictive assumption; it merely determines the outlier detection technique implemented during the validation and diagnostics stages (see below), and for which several variants are admissible.

The steps involved in the training stage are summarized as follows (see also Figure 2):

[**T1**] Decide on the number n of the monitored vibration modes.
[**T2**] Collect MSC data over a number of τ_q distinct long-term scale temporal points.
[**T3**] From the set $\mathcal{T}(\tau)$, extract a representative estimation subset, $\mathcal{T}_e(\tau)$.
[**T4**] Construct the data matrices $\mathbf{D}_j$ for $j = 1, 2, \ldots, n$.

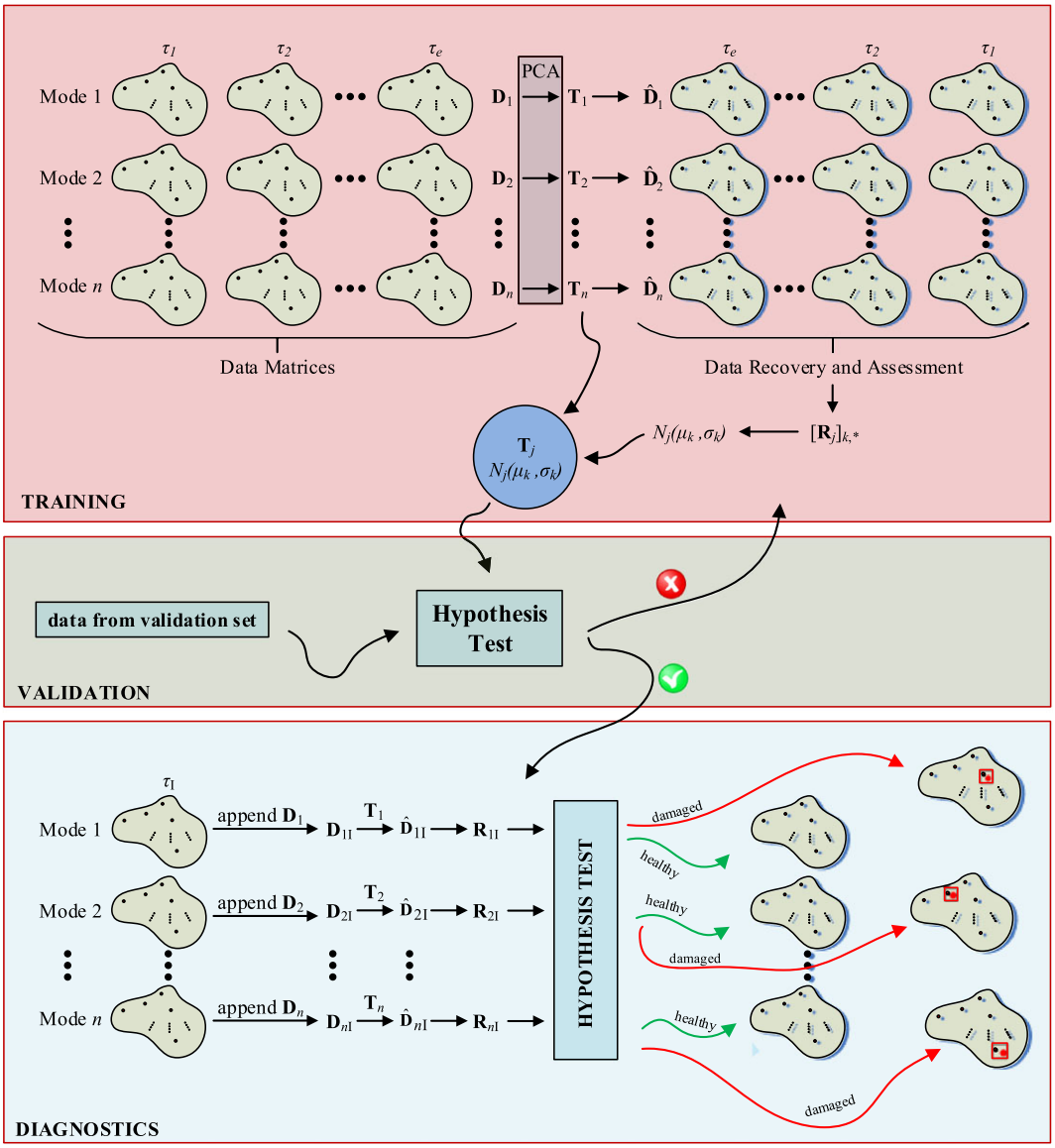

FIGURE 2 Training and diagnostics stages of the proposed damage localization process

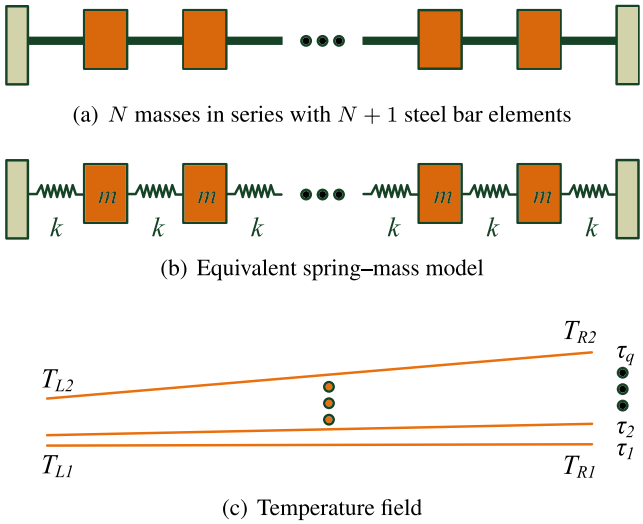

(a) N masses in series with $N+1$ steel bar elements

(b) Equivalent spring–mass model

(c) Temperature field

FIGURE 3 Case study I: temperature-dependent structural system in horizontal vibration

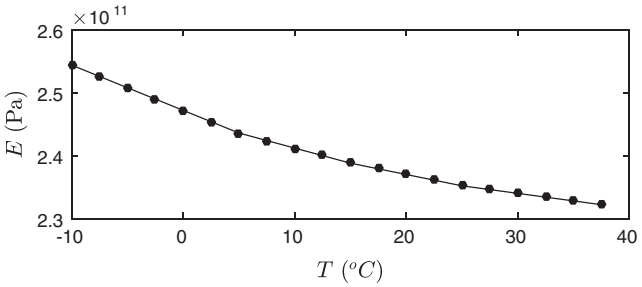

FIGURE 4 Young's modulus of steel versus temperature

TABLE 1 Structural and environmental parameters for the structure of Figure 3 (Case study I)

Parameter	Value	Unit
N	49	-
m	30	kg
L	0.30	m
A	2.83×10^{-5}	m^2
T_{L1}	-10	°C
T_{L2}	20	°C
T_{R1}	-10	°C
T_{R2}	40	°C
ΔT_R	0.5	°C
τ_q	101	-

[**T5**] Perform PCA and extract the loading matrices $\mathbf{T}_j$.

[**T6**] Calculate the residual matrices $\mathbf{R}_j$.

[**T7**] Perform statistical characterization of the sample row vectors $[\mathbf{R}_j]_{k,*}$ and estimate the $N_j(\mu_k, \sigma_k^2)$ distributions, for $k = 1, 2, \ldots, p$.

The output of the training process contains the loading matrices $\mathbf{T}_j$ and the $N_j(\mu_k, \sigma_k^2)$ distributions for every mode and every node of the structure. Prior to adopting these quantities for the diagnostics process, a verification step is implemented on the MSC data from the long-term scale temporal points of the validation set $\mathcal{T}_v(\tau)$. The steps involved are

identical to these of the diagnostics stage overviewed next, so they are not listed here for brevity. It must be noted that, as Figure 2 indicates, if the validation results are unsuccessful the training stage must be revisited in terms of the training points and the adopted normality assumption. On the contrary, if validation proves successful, the estimated quantities may be subsequently used for the diagnostics stage.

This stage pertains to the MSC data matrix established at a long-term temporal point τ_{I}, where damage might have occurred. This new data may be appended to the existing $\mathbf{D}_j$ matrices as trailing columns, that is,

$$\mathbf{D}_{j\mathrm{I}} = [\mathbf{D}_j, \mathbf{W}_j], \quad j = 1, 2, \ldots, n, \tag{14}$$

where $\mathbf{W}_j = [\Psi_j(\tau_{\mathrm{I}}, 1), \ldots, \Psi_j(\tau_{\mathrm{I}}, p)]^T$. Using the loading matrices of the training stage and Equation 12, projection and re-mapping of $\mathbf{D}_{j\mathrm{I}}$ reads

$$\widehat{\mathbf{D}}_{j\mathrm{I}} = \mathbf{T}_j^T \mathbf{T}_j \mathbf{D}_{j\mathrm{I}} \tag{15}$$

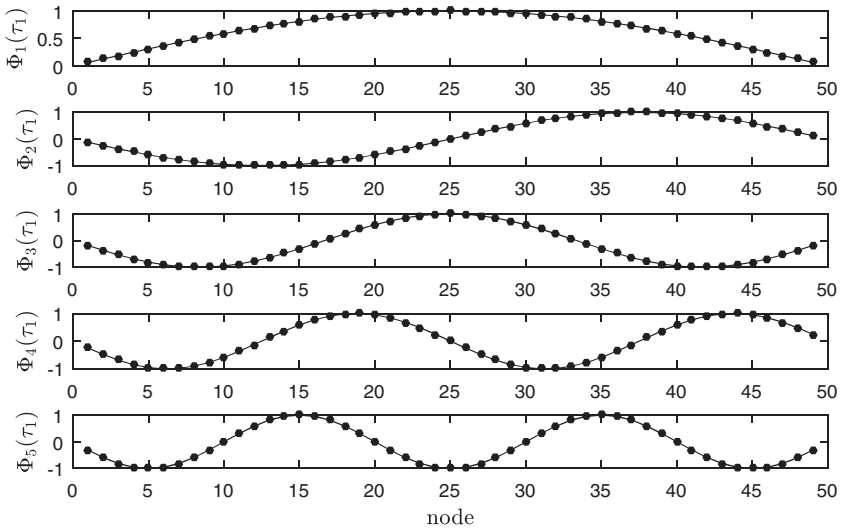

FIGURE 5 First five normalized mode shapes of the structure at τ_1. The relative position of every node has been arranged vertically for convenience (Case study I)

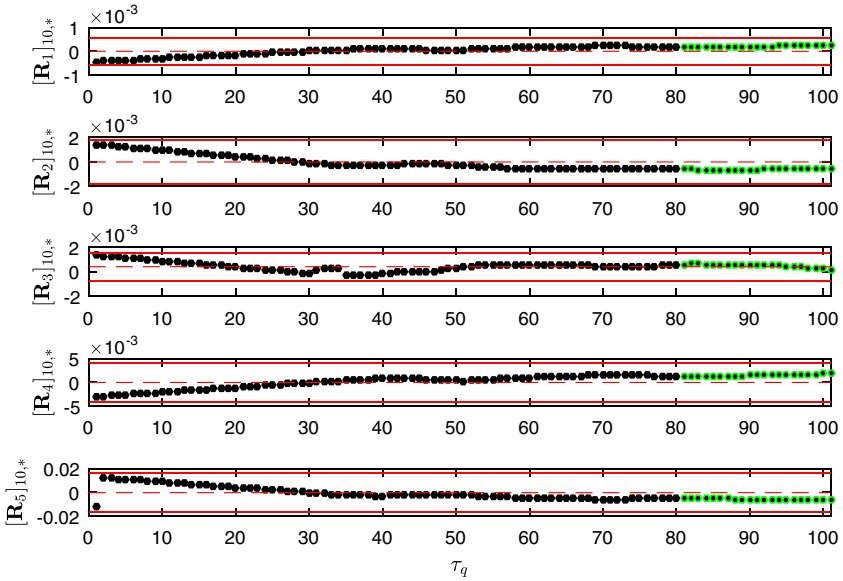

FIGURE 6 Training and validation stages: samples of the residual matrix at Node 10 for the first five vibration modes. The black dots correspond to the long-term scale temporal points of the estimation set $\mathcal{T}_e(\tau)$, and the green dots to the ones of the validation set $\mathcal{T}_v(\tau)$. The red dashed line corresponds to the mean value μ of the estimation samples (e.g., the black dots) and the red continuous lines to $\mu \pm 3\sigma$, where σ is the standard deviation of the estimation samples (Case study I)

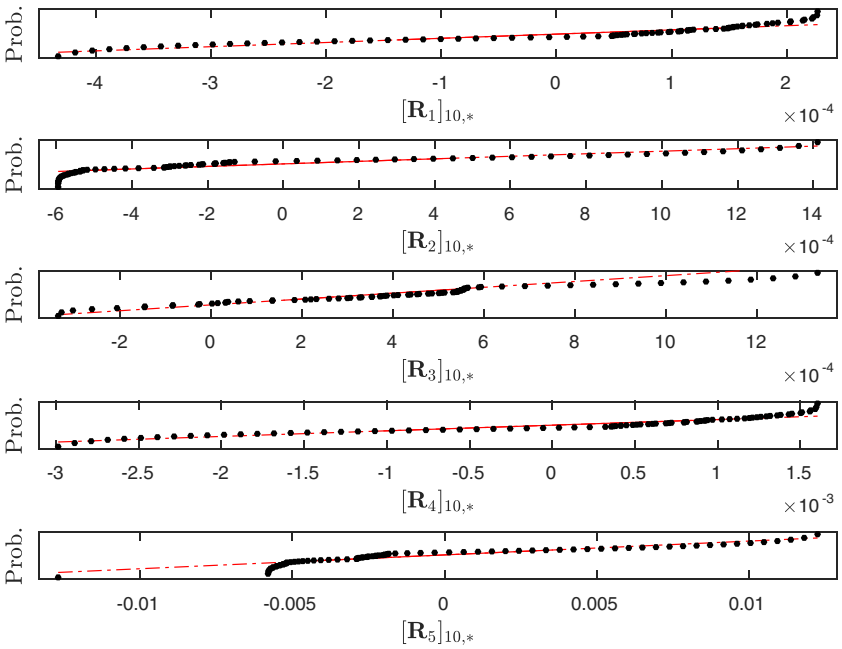

FIGURE 7 Training stage: normal probability plots for the estimation samples of Figure 6 (Case study I)

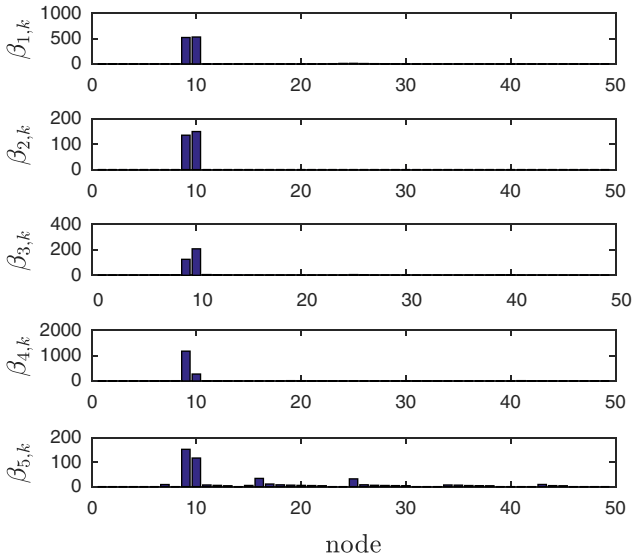

FIGURE 8 Diagnostics stage: damage index for 15% damage in Bar element 10 (Case study I)

and the updated residual matrix is retrieved as

$$\mathbf{R}_{j\mathrm{I}} = \mathbf{D}_{j\mathrm{I}} - \widehat{\mathbf{D}}_{j\mathrm{I}}. \tag{16}$$

The difference between $\mathbf{R}_j$ as defined in Equation 13 and $\mathbf{R}_{j\mathrm{I}}$ appearing in Equation 16 is that the latter contains one additional sample in every row. It hence should be determined whether this sample complies with the estimated distribution of this row, $N_j(\mu_k, \sigma_k^2)$, or whether it in fact originates from an unmodelled source, such as damage. This is a typical univariate single outlier detection problem, which may be addressed using Grubbs' test,[72] provided the data is approximately normal. If this is not the case, then alternative tests should be considered (e.g., the Walsh test). Grubbs' test is briefly reviewed in the Appendix A. In the herein adopted version, the Grubbs' two-sided test statistic G is compared to the critical Grubbs value G_{cr} (for an upper one-tailed test), at a certain significance level α. If $G < G_{cr}$, the null hypothesis (e.g., no outliers are contained in the data) is adopted, otherwise the alternative hypothesis (e.g., outliers are contained in the data) is adopted instead. A damage index may then be defined in terms of the distance of the new sample from the

mean value of the corresponding distribution

$$\beta_{j,k} = \begin{cases} 0 & G < G_{cr} \\ \frac{|[\mathbf{R}_j]_{k,\tau_1}|}{\sigma_k} & G > G_{cr}, \end{cases} \tag{17}$$

for $j = 1, 2, \ldots, n$ and $k = 1, 2, \ldots, p$. The reason for formulating the damage index of Equation 17, instead of adopting the pure G statistic and a simple Boolean zero-one decision pattern, is that the underlying mechanisms of structural damage are often complex, with damage in one location bearing effects, and associated outliers, in further locations along the structure. It must be further emphasized that there is no guarantee that under a specific damage, the same index is "excited" in all monitored modes, implying that a damage may be sensitive in only a subset of particular higher order modes. As Figure 2 indicates, damage may "hit" at different points of the MSCs, or may not be captured at all.

To conclude, the diagnostics stage comprises the following steps:

[**I1**] Gather MSC data at a long-term scale temporal point τ_{I}.
[**I2**] Construct the data matrices $\mathbf{D}_{j\mathrm{I}}$ for $j = 1, 2, \ldots, n$ as in Equation 14.

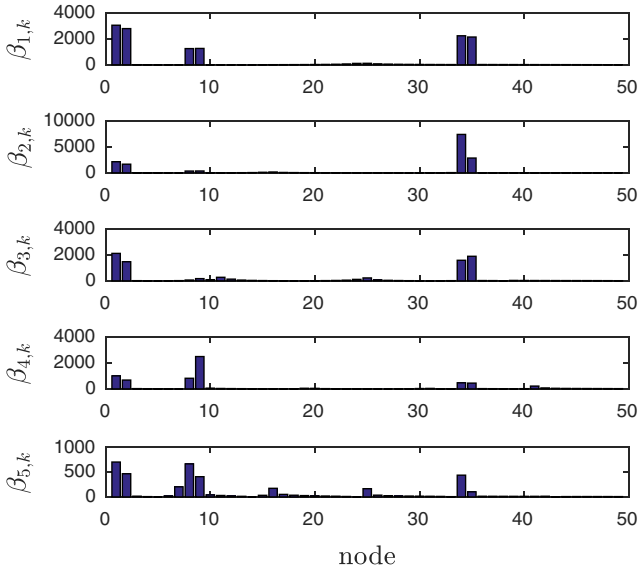

FIGURE 9 Diagnostics stage: damage index for damages at random positions and of random amplitudes along the structure (Case study I)

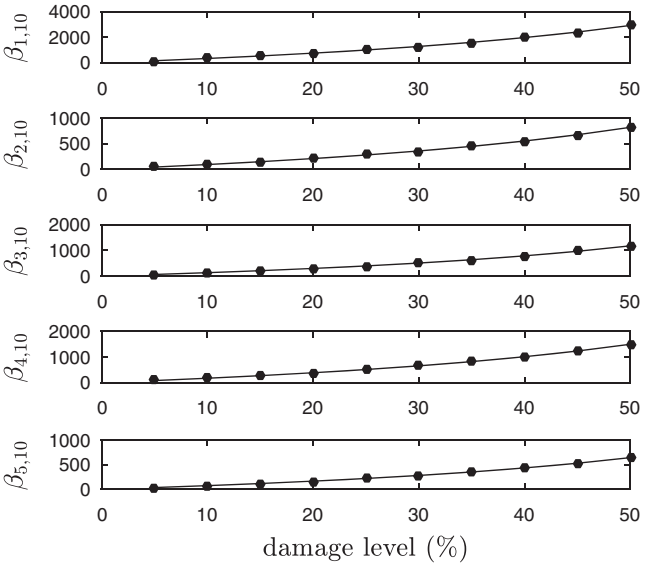

FIGURE 10 Damage index versus damage level in Bar element 10 for the first five vibration modes of the structure (Case study I)

[**I3**] Calculate the residual matrices $\mathbf{R}_{j1}$.
[**I4**] Perform hypothesis testing for the extended row vectors of $\mathbf{R}_{j1}$.
[**I5**] Estimate the $\beta_{j,k}$ metric across monitored nodes and for all modes considered.
[**I6**] Assess/decide on the current state of the structure.

3 | CASE STUDIES

3.1 | A spring–mass chain model

The proposed scheme is now applied to the damage detection and localization problem of the simulated, temperature-dependent structural system of Figure 3(a). The structure consists of a series of masses that are interconnected with steel bar elements, which are characterized by length L, cross-sectional area A, and *nonlinear*

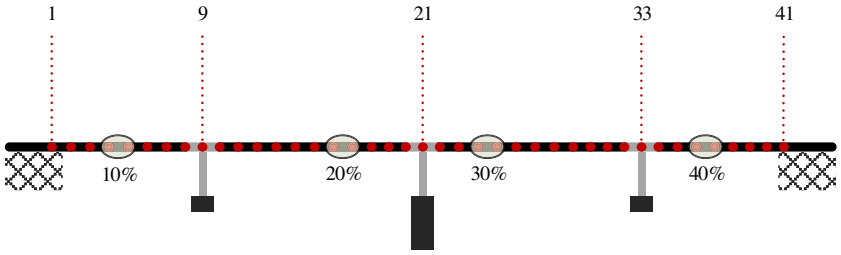

FIGURE 11 Case study II: a 4-span bridge structure

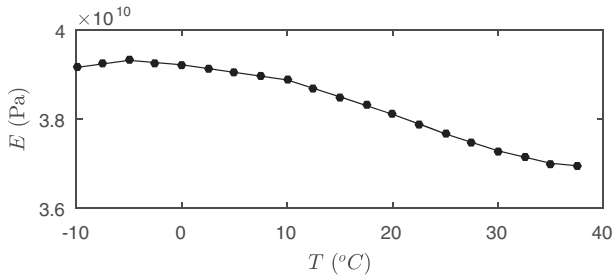

FIGURE 12 Young's modulus of concrete versus temperature

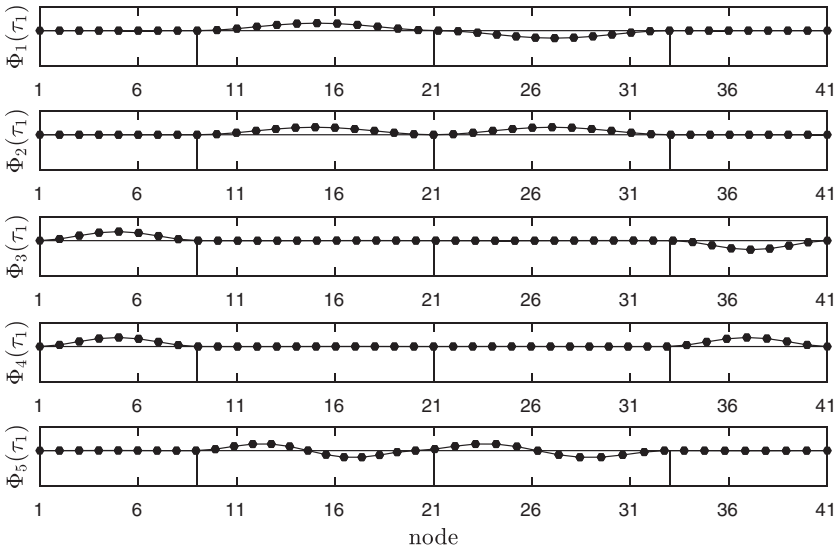

FIGURE 13 First five mode shapes of the bridge at τ_1 (Case study II)

temperature-dependent modulusE as specified in Figure 4. An equivalent mechanical system is approximated, as shown in Figure 3(b) with springs of stiffness k equal to EA/L, while damage is introduced in the form of diverse levels of modulus reduction in specific bar elements, ranging from 5% to 50%. Table 1 lists the adopted numerical values for the underlying parameters.

As illustrated in Figure 3(c), the structure is exposed to temperature variations along its length with the temperature of the far right bar, henceforth referred to as the reference temperature, varying between T_{R1} and T_{R2}, whereas the temperature on the far left varies between T_{L1} and T_{L2}. A linear interpolation is assumed for the temperatures of the intermediate bar elements (Figure 3(c)). Under this setting, $\tau_q = 101$ distinct structural realizations are carried out at different values of the reference temperature (see Table 1). For the first temperature curve, the one that refers to long-term scale τ_1 and corresponds to reference temperature $T_{R1} = -10$ °C and far left bar temperature $T_{L1} = -10$ °C (e.g., with no temperature gradient), Figure 5 displays the first five normalized mode shapes of the structure, where the relative motions of the nodes are represented vertically (instead of horizontally), in order to better visualize the induced modal behavior.

Upon establishing that $d = 1$ is appropriate for the adequate description of the operational variability, Figures 6, 7 illustrate the results of the training and validation stages on Node 10 of the structure, whose behavior is characteristic

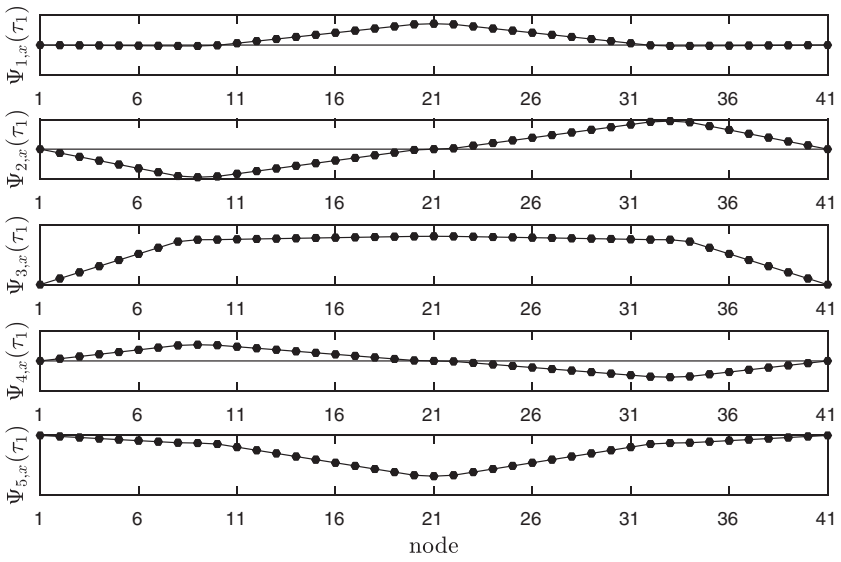

(a) horizontal direction

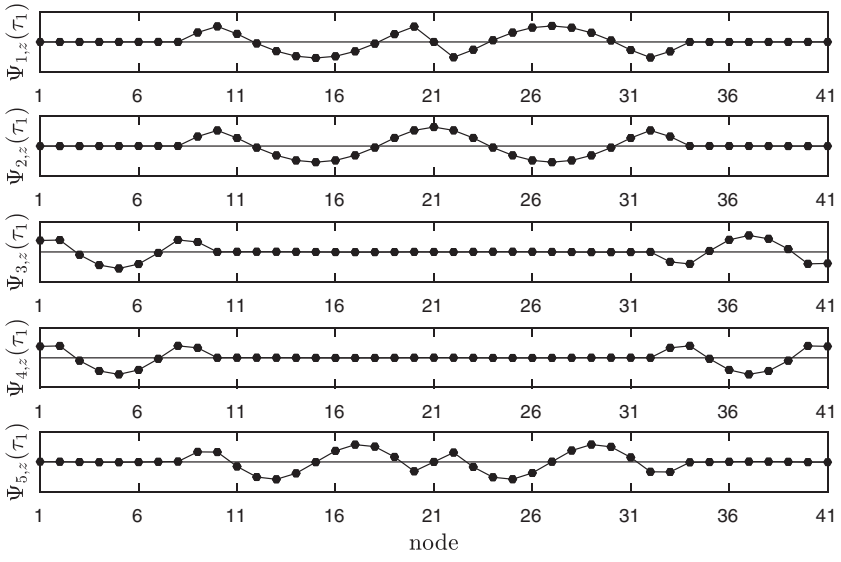

(b) vertical direction

FIGURE 14 Mode shape curvatures of the bridge at τ_1 (Case study II)

of all the other nodes examined. Figure 6 demonstrates the samples of the $[\mathbf{R}_j]_{10,*}$ vectors for the estimation set $\mathcal{T}_e(\tau)$, comprising the first 80 temporal points of the training set $\mathcal{T}(\tau)$. All values are contained within the $\mu \pm 3\sigma$ confidence intervals, whereas the normal probability plots of Figure 7 confirm the assumption of approximate normality and qualify Grubbs' test as appropriate. This is further supported in the validation stage, where the appended samples of the validation set $\mathcal{T}_v(\tau)$ are bounded by the same statistics, returning zero-valued damage indices.

In the diagnostics stage, Figure 8 plots the damage indices calculated at every mode for a single damage (15% modulus reduction) at Bar element 10. The damage has been quite accurately detected and localized, returning sufficiently high values of $\beta_{j,9}$ and $\beta_{j,10}$ for Nodes 9 and 10, respectively (e.g., the neighboring nodes of the damaged bar element). One may also observe the presence of nonnegligible damage indices in further nodes, particularly in the last mode. Although these values do correspond to outliers of the diagnostics residual matrix in these locations, they may not be considered

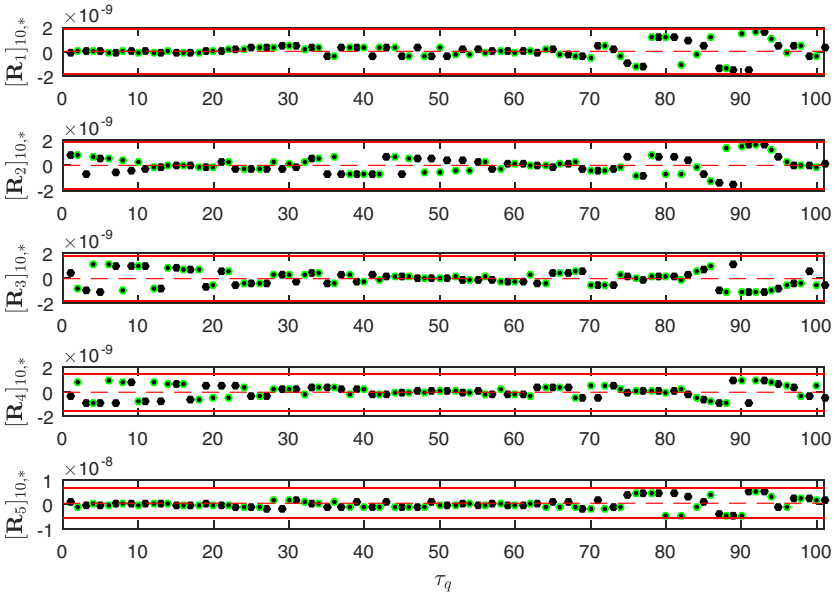

(a) Samples of the residual matrix. Black dots correspond to the long-term scale temporal points of the estimation set $\mathcal{T}_e(\tau)$ and green dots to the validation set $\mathcal{T}_v(\tau)$. The red dashed line corresponds to the mean value μ of the estimation samples (e.g. the black dots) and the red continuous lines to $\mu \pm 3\sigma$, where σ the standard deviation of the estimation samples

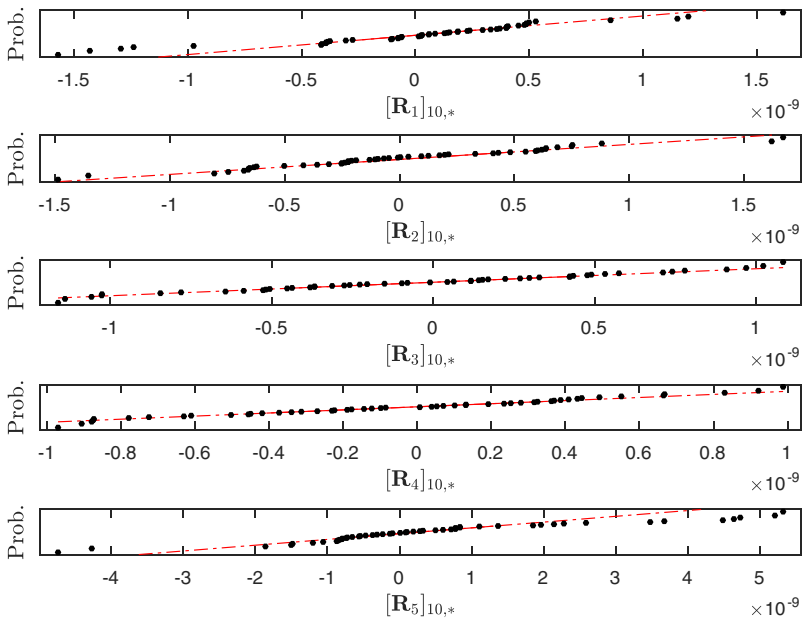

(b) Normal probability plots for the estimation samples of the figure above

FIGURE 15 Training and validation stages: performance of the residual matrix at Node 15 in horizontal direction (Case study II)

as significant indications of damage in the respective nodes. Instead, these are attributed to the normality assumption for the rows of the residual matrices at these locations. An increase in the dimension d may be one way to deal with this issue.

The case of multiple simultaneous damages is also considered in this case study. Figure 9 illustrates the results for three damages randomly imposed on the structure, both in terms of position (Bar elements 2, 9, and 35) and in terms of amplitude (40%, 30%, and 45%, respectively). All damages have been successfully detected and localized, albeit localization is not apparent across all modes. For instance, in the third mode, the damage in Bar element 9 is hardly visualized, while for the fourth mode the damage in Bar element 35 is not clearly picked up. It is further observed that the values of the indices among damaged nodes are not consistent. For example, the severity of damage in Bar element 9 is lower (30%) than the one in Bar element 35 (45%), yet in the fourth mode, the damage index at Node 9 is sufficiently higher than the one of Nodes 34–35. This observation is expected as damage bears different effects to different modes. Although this

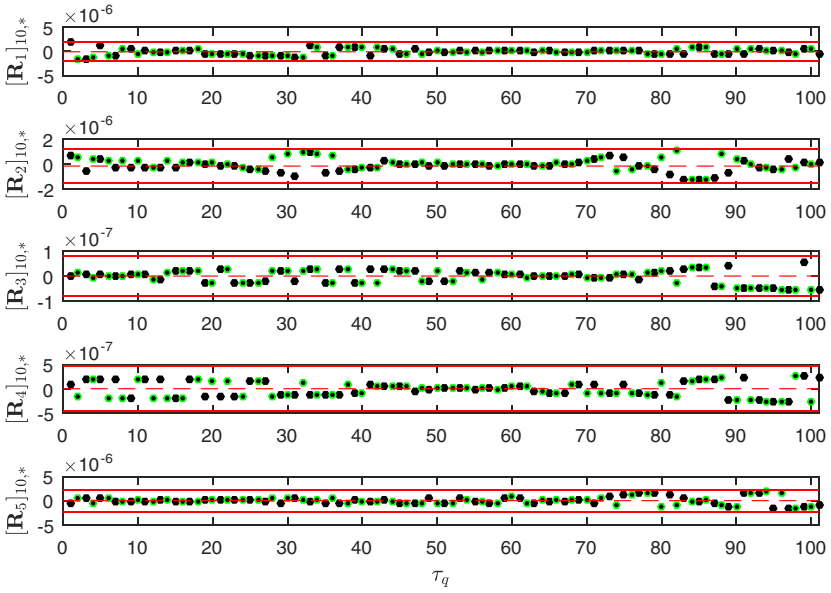

(a) Samples of the residual matrix. Black dots correspond to the long-term scale temporal points of the estimation set $\mathcal{T}_e(\tau)$ and green dots to the validation set $\mathcal{T}_v(\tau)$. The red dashed line corresponds to the mean value μ of the estimation samples (e.g. the black dots) and the red continuous lines to $\mu \pm 3\sigma$, where σ the standard deviation of the estimation samples

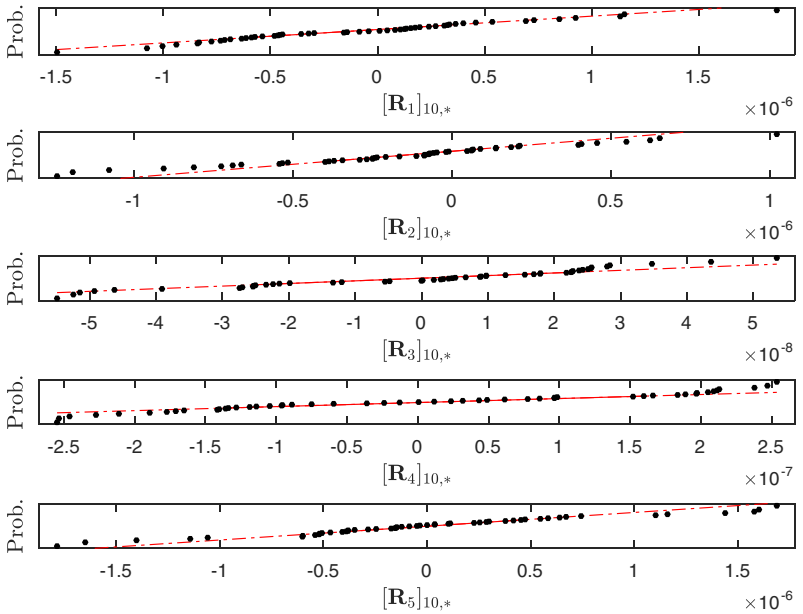

(b) Normal probability plots for the estimation samples of the figure above

FIGURE 16 Training and validation stages: performance of the residual matrix at Node 15 in vertical direction (Case study II)

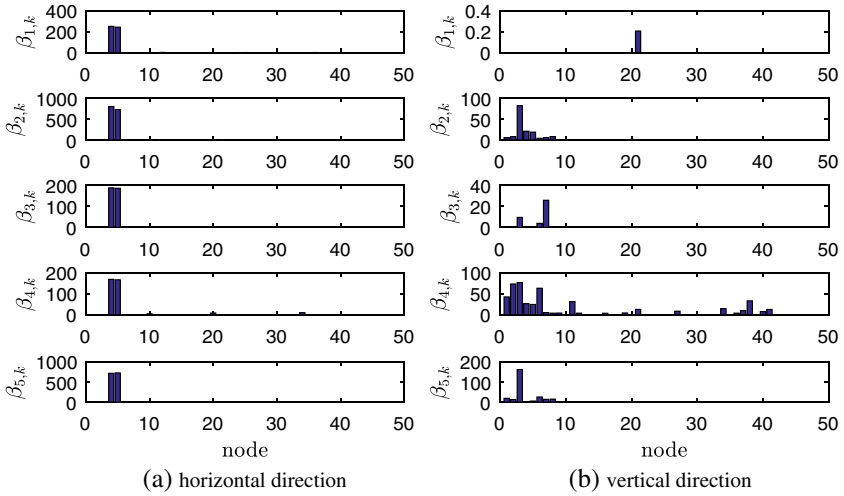

(a) horizontal direction (b) vertical direction

FIGURE 17 Diagnostics stage: damage index for 10% damage in Bar element 4 (Case study II).

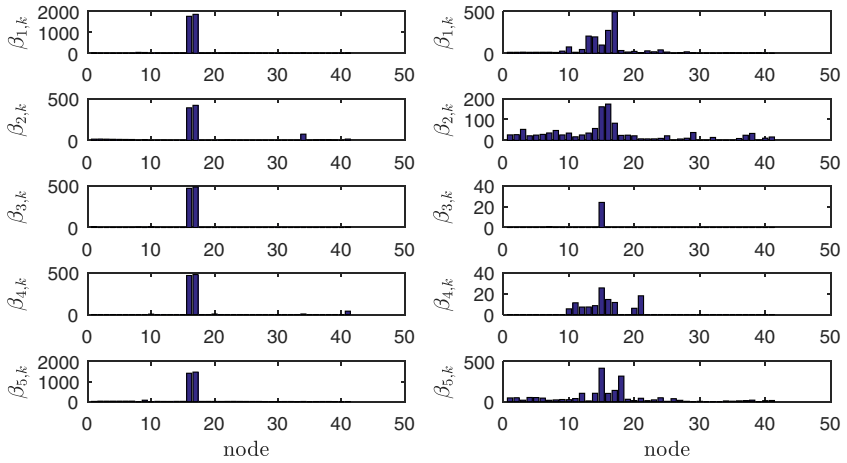

(a) horizontal direction (b) vertical direction

FIGURE 18 Diagnostics stage: damage index for 20% damage in Bar element 17 (Case study II)

issue may be tackled with availability of a model, and classification of expected damage patterns, this study indicates that substantial evidence may be collected on the basis of output-only data alone.

The former observation raises the question of whether the damage index of Equation 17 can be correlated to the damage severity. Returning to Bar element 10, the indices for different damage levels, ranging from 5% to 50%, have been calculated and displayed in Figure 10 for the first five modes. The correlation between the damage index and the damage severity is quite obvious for all modes, yet the same damage level does not return the same index value in all modes.

3.2 | A 4-span bridge

The second case study pertains to the damage localization problem of the simulated 4-span bridge model illustrated in Figure 11, which corresponds to a modified version of the one presented in Yan et al.[58] and here serves for benchmarking purposes. The bridge is discretized in 41 nodes and 40 beam elements, 8 of which are concrete (e.g., 2 around each intermediate support). Environmental variations of the bridge are taken into account by introducing temperature-dependent Young modulus for steel and concrete, as shown at Figures 4 and 12. The bridge is additionally exposed to temperature variations along its length, as in the previous case study, with the reference temperature varying between $T_{L1} = -10$ °C and $T_{L2} = 40$ °C and the left between $T_{R1} = -10$ °C and $T_{R2} = 0$ °C. A linear interpolation between the two ends is assumed for the temperature of the intermediate nodes along the bridge (Figure 3(c) and Table 1). The first five mode shapes of the bridge at τ_1 (e.g., no temperature gradient) are displayed in Figure 13, where it is observed that (a) each

mode is locally excited in only two of the four spans and (b) the relative motion of the nodes in the horizontal direction is negligible compared to the one in the vertical direction. Yet Figure 14 reveals that the directional MSCs retain significant information in both directions and they should be equally considered for damage detection and localization.

Damage is again introduced as local modulus reductions in specific positions (see Figure 11), namely, 10% in Bar element 4 (Nodes 4 and 5, Span 1), 20% in Bar element 17 (Nodes 16 and 17, Span 2), 30% in Bar element 25 (Nodes 24 and 25, Span 3), and 40% in Bar element 37 (Nodes 36 and 37, Span 4). Under this setting, 101 distinct realizations are carried out for different values of the reference temperature. Out of these, the odd and the even temporal points compose the training and the validation sets, $\mathcal{T}_e(\tau)$ and $\mathcal{T}_v(\tau)$, respectively.

In order to determine dimension d for each direction, a number of values are examined and the final selection is made in accordance to the quality of the induced normal probability plots over a number of nodes. Dimensions of $d = 1$ for the horizontal and $d = 2$ for the vertical direction are selected as appropriate. Figures 15, 16 display the results of the training and the validation stages for an indicative node (Node 15) in both directions. The training and the validation subsets exhibit quite standard behavior, with the former returning good approximations to the normal distribution and the latter being constrained within the 99.7% distribution limits, returning zero damage indices.

Having established a statistically sound training stage for the bridge in its healthy state, the results of the diagnostics stage are expanded individually for each damage over Figures 17 –20. The behavior of the damage index leads to some interesting remarks. In the case of the first damage (e.g., 10% damage in Bar element 4, see Figure 17), a very accurate detection and localization result occurs in horizontal direction (Figure 17(a)). The indices of the two neighboring nodes

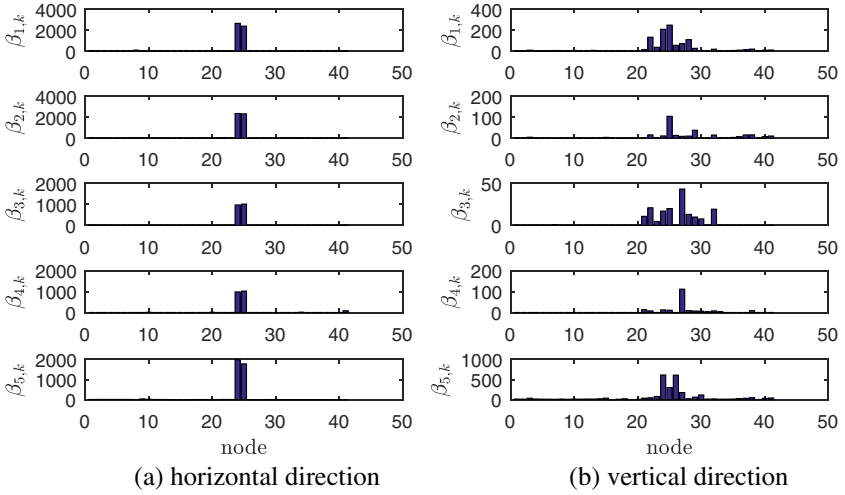

(a) horizontal direction (b) vertical direction

FIGURE 19 Diagnostics stage: damage index for 30% damage in Bar element 25 (Case study II)

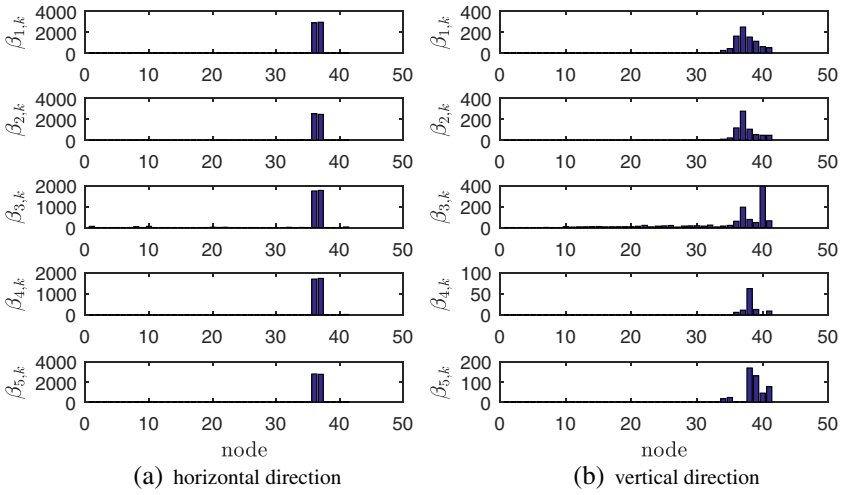

(a) horizontal direction (b) vertical direction

FIGURE 20 Diagnostics stage: damage index for 40% damage in Bar element 37 (Case study II)

of the damaged bar element have returned sufficiently high values in all monitored modes, whereas the values of all other nodes are essentially zero. On the contrary, a mixed behavior is observed in the vertical direction (Figure 17(b)), where damage is rather detected (Modes 2 and 5), almost detected (Mode 4), or not detected at all (Modes 1 and 3). This behavior is partially attributed to the shape of the MSCs at the vertical direction and the point of damage (see Figure 14(b)) in conjunction with the relatively low damage level. It is noted that higher values of d do not improve the performance: On the contrary, they produce rather "noisy" damage indices.

The performance of the proposed methodology in all other individual damages is quite similar: The damage is very accurately detected and localized in the horizontal direction (left plots of Figures 18 –20), whereas it is detected but only partially localized in the vertical direction (left plots of Figures 18 –20), although the behavior of the latter is significantly better. This is however expected, because (a) the damages are of higher severity and (b) the locations are more "informative" in terms of mode shape and MSC behavior (Figures 13 and 14(b)). Nonetheless, it appears that these damages produce a cloud of indices around the exact location in the vertical direction, rendering the detection successful and the localization partially successful, at least in comparison to their horizontal counterparts.

Figure 21 illustrates the calculated indices for both directions when all damages are included in the same diagnostics stage. The aforementioned comments are obviously valid here as well, and it is interesting to observe that the values of the damage indices in the horizontal direction almost precisely follow the damage severity in most of the vibration modes. It can be therefore argued that the effects of the underlying damages result as rather distributed along the vertical direction, while they remain dominantly local along the horizontal.

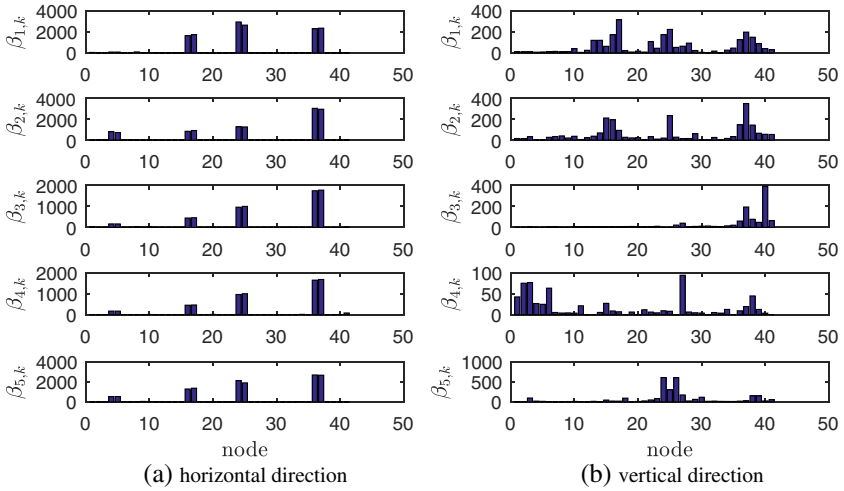

(a) horizontal direction (b) vertical direction

FIGURE 21 Diagnostics stage: damage index for multiple damages (Case study II)

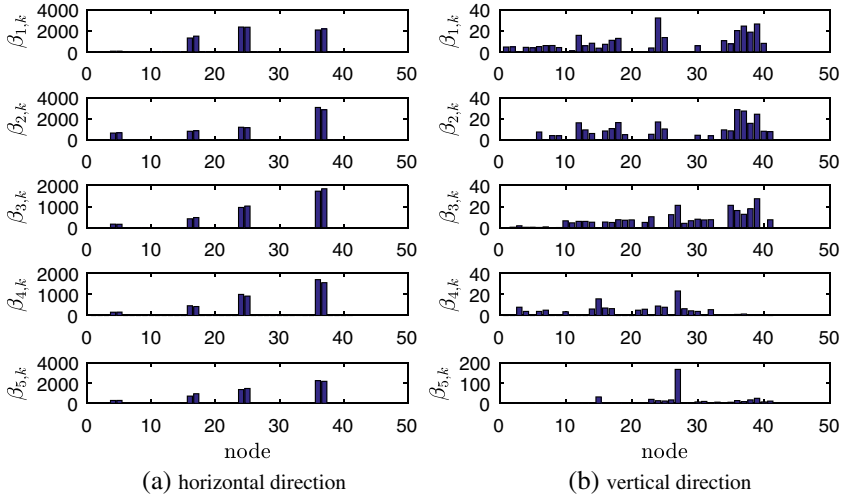

(a) horizontal direction (b) vertical direction

FIGURE 22 Diagnostics stage: damage index for multiple damages and noise-corrupted mode shape curvatures (Case study II)

A final remark pertains to the case of noise-corrupted data. Figure 22 contains the same information as Figure 21, only now the MSCs have been corrupted with Gaussian white noise, by superimposing an independent random value to each MSC vector entry, of zero mean and standard deviation that is 5% of the value of that entry. From Figure 22(a), it follows that the damage index maintains the same behavior along the horizontal direction, returning values with slightly lower amplitudes, whereas in the vertical direction (Figure 22(b)), the "noisy" behavior previously mentioned is rather amplified along the length of the bridge. This indicates that the damage index exhibits increased robustness against data contamination.

4 | CONCLUSION

This paper introduces a PCA-based method for addressing the challenges in the damage detection and localization process caused by varying environmental conditions. The developed procedure distinguishes between variations induced due to environmental influences and changes induced by damage or deterioration. In the case of linear or weakly nonlinear behavior, the proposed method is successful in discerning between damaged and intact structural data sets. A training stage is required on the healthy, or baseline system, in order to capture the influence of environmental and operational effects in the response features and to accurately represent these via a PCA transformation. During the diagnostics stage, the residual between the original and approximated MSC features is exploited to form a damage index on the basis of a simple hypothesis test. Values of this index above an acceptable threshold serve for damage detection and localization. A significant advantage of the proposed method is that it is output-only, that is, it requires no explicit measurement of environmental or operational parameters, obviating many practical hindrances. The presented numerical case studies indicate good performance both in terms of detection and in terms of localization, with quantification posing somewhat of a challenge. Engineering judgment may serve in addressing the latter issue, because a particular type of damage will often bear more pronounced effects on specific modes, which would imply that quantification ought be sought on the basis of specific modal subsets as opposed to the entire modal set. A major contribution of this study lies in demonstrating that substantial evidence towards all four levels of the SHM process (detection, localization, quantification, and decision) may be collected on the basis of output-only monitoring data.

ACKNOWLEDGEMENT

Prof. E. Chatzi would like to gratefully acknowledge the support of the Albert Lück foundation.

ORCID

Vasilis K. Dertimanis http://orcid.org/0000-0002-4671-1962
Eleni N. Chatzi http://orcid.org/0000-0002-6870-240X

REFERENCES

[1] D. Balageas, in *Structural Health Monitoring*, (Eds: D. Balageas, C.-P. Fritzen, A. Güemes), chap. 1, ISTE, London, UK **2006**, 13–43.
[2] P. Chang, A. Flatau, S. Liu. *Struct. Health Monit.* **2003**, *2*(3), 257.
[3] H. Wenzel, *Health Monitoring of Bridges*, John Wiley & Sons, New York, USA **2008**.
[4] C. Farrar, K. Worden. *Philos. Trans. R. Soc. London A Math Phys Eng Sci* **2007**, *365*(1851), 303.
[5] A. Teughels, G. De Roeck. *J. Sound Vib.* **2004**, *278*(3), 589.
[6] J. Maeck, B. Peeters, G. De Roeck. *Smart Mater. Struct.* **2001**, *10*(3), 512.
[7] A. Rytter, Vibrational based inspection of civil engineering structures, *PhD Thesis*, Department of Building Technology and Structural Engineering, Aalborg University, Aalborg, Denmark **1993**. http://vbn.aau.dk/en/publications/vibrational-based-inspection-of-civil-engineering-structures(4d0b4f40-c6e9-11de-bcee-000ea68e967b).html
[8] E. Carden, P. Fanning. *Struct. Health Monit.* **2004**, *3*(4), 355.
[9] G. Busca, M. P. Limongelli. *J. Civil Struct. Health Monit.* **2015**, *5*(4), 427.
[10] Y. Yan, L. Cheng, Z. Wu, L. Yam. *Mech. Syst. Signal Process.* **2007**, *21*(5), 2198.
[11] C. Farrar, S. Doebling, in *Proceedings of EUROMECH 365 International Workshop: DAMAS 97, Structural Damage Assessment using Advanced Signal Processing Procedures*, Sheffield, UK **1997**, 269.

[12] S Doebling, C Farrar, M Prime, D Shevitz, Damage identification and health monitoring of structural and mechanical systems from changes in their vibration characteristics: a literature review, *Technical Report*, Report Number LA-13070-MS. Los Alamos National Laboratory, NM, US **1996**.

[13] H. Sohn, C Farrar, F Hemez, D Shunk, D Stinemates, B Nadler, J Czarnecki, A review of structural health monitoring literature: 1996-2001, *Technical Report*, Report Number LA-13976-MS. Los Alamos National Laboratory, NM, US **2004**.

[14] M. P. Limongelli, E. Chatzi, M. Döhler, G. Lombaert, E. Reynders. in *8th European Workshop On Structural Health Monitoring (EWSHM 2016)*, July 5-8, **2016**, Bilbao, Spain.

[15] F. Catbas, M. Gul, J. Burkett. *Mech. Syst. Signal Process.* **2008**, *22*(7), 1650.

[16] F. Catbas, A. Aktan. *J. Struct. Eng.* **2002**, *128*(8), 1026.

[17] A. Aktan, F. Catbas, K. Grimmelsman, C. Tsikos. *J. Eng. Mech.* **2000**, *126*(7), 711.

[18] R. C. George, J. Posey, A. Gupta, S. Mukhopadhyay, S. K. Mishra, *Damage Detection in Railway Bridges under Moving Train Load*, Springer International Publishing, Cham **2017**. 349.

[19] M. Çelebi, A. Sanli, M. Sinclair, S. Gallant, D. Radulescu. *Earthquake Spectra* **2004**, *20*(2), 333.

[20] P. Cornwell, C. Farrar, S. Doebling, H. Sohn. *Exp. Tech.* **1999**, *23*(6), 45.

[21] C. Liu, J. De Wolf. *J. Struct. Eng.* **2007**, *133*(12), 1742.

[22] R. Rohrmann, M. Baessler, S. Said, W. Schmid, W. Ruecker, in *Proceedings of IMAC XVI - 18th International Modal Analysis Conference*, San Antonio, TX, USA **2000**, article no. 141.

[23] C. Farrar, S. Doebling, P. Cornwell, E. Straser, in *Proceedings of IMAC XV - 15th International Modal Analysis Conference*, Orlando, FL, USA. **1997**, 257.

[24] S. Alampalli. *Mech. Syst. Signal Process.* **2000**, *14*(1), 63.

[25] B. Peeters, Guido De Roeck. *Earthquake Eng. Struct. Dyn.* **2001**, *30*(2), 149.

[26] E. Cross, K. Koo, J. Brownjohn, K. Worden. *Mech. Syst. Signal Process.* **2013**, *35*(12), 16.

[27] V. Meruane, W. Heylen, in *Proceedings of ISMA2010: International Conference on Noise and Vibration Engineering*, Leuven, Belgium. **2010**, 1463.

[28] G. Feltrin, in *Proceedings of 4th International Conference on Structural Dynamics, Eurodyn 2002*, Munich, Germany. **2002**, 373.

[29] S. Alampalli, in *Proceedings of IMAC XVI - 16th International Modal Analysis Conference*, Santa Barbara, Ca, US. **1998**, 111.

[30] V. Meruane, W. Heylen. *Struct. Health Monit.* **2012**, *11*(3), 345.

[31] M. Basseville, F. Bourquin, L. Mevel, H. Nasser, F. Treyssede. *J. Eng. Mech.* **2010**, *136*(3), 367.

[32] V. Nguyen, J. Mahowald, J. Golinval, S. Maas, in *Proceedings of EURODYN 2014: 9th International Conference on Structural Dynamics*, Porto, Portugal. **2014**, 2613.

[33] C. Oh, H. Sohn. *J. Sound Vib.* **2009**, *325*(1), 224.

[34] M. Spiridonakos, E. Chatzi, B. Sudret. *ASCE-ASME J. Risk Uncertainty Eng. Syst. Part A: Civil Eng.* **2016**, *2*(3), B4016003.

[35] W. Hu, S. Thöns, R. Rohrmann, S. Said, W. Rücker. *Eng. Struct.* **2015**, *89*, 273.

[36] H. Sohn. *Philos. Trans. R. Soc. London A: Math. Phys. Eng. Sci.* **2007**, *365*(1851), 539.

[37] V. Nguyen, J. Mahowald, S. Maas, J. Golinval, in *Proceedings of the Fifth IEEE International Conference on Communications and Electronics*, Danang, Vietnam **2014**.

[38] N. Dervilis, K. Worden, E. Cross. *J. Sound Vib.* **2015**, *347*, 279.

[39] M. Spiridonakos, E. Chatzi. *Comput. Struct.* **2015**, *157*, 99.

[40] F. Magalhães, A. Cunha, E. Caetano. *Mech. Syst. Signal Process.* **2012**, *28*, 212.

[41] J. Ko, K. Chak, J. Wang, Y. Ni, T. Chan, in *Proceedings of SPIE 5057: Smart Structures and Materials 2003: Smart Systems and Nondestructive Evaluation for Civil Infrastructures*, San Diego, CA, USA. **2003**, 298.

[42] J. Kullaa, in *Proceedings of the 1st European Workshop on Structural Health Monitoring*, Paris, France. **2002**, 742–749.

[43] D. Bernal, in *Sensor Technologies for Civil Infrastructures*, vol. 2, (Eds: M. Wang, J. Lynch, H. Sohn), Woodhead Publishing, Cambridge, UK **2014**, 67–92.

[44] E. Figueiredo, G. Park, C. Farrar, K. Worden, J. Figueiras. *Struct. Health Monit.* **2011**, *10*(6), 559–572.

[45] Y. Harmanci, M. Spiridonakos, E. Chatzi, W. Kübler. *Front. Built Environ.* **2016**, *2*, 13.

[46] H. Sohn, K. Worden, C. Farrar, in *Proceedings of SPIE4330: 8th Annual International Symposium on Smart Structures and Materials*, Newport Beach, CA, USA. **2001**, 108.

[47] N. Dervilis, M. Choi, S. Taylor, R. Barthorpe, G. Park, C. Farrar, K. Worden. *J. Sound Vib.* **2014**, *333*(6), 1833.

[48] V. Lämsä, J. Kullaa, in *Proceedings of the 6th International Workshop on Structural Health Monitoring*, (Eds: F-K Chang), Stanford University, DEStech Publications, Stanford, CA. **2007**, 1092.

[49] G. Manson, in *Proceedings of the 3rd International Conference on Identification in Engineering Systems*, Swansea, UK. **2002**, 187.

[50] K. Person. *Philos. Mag.* **1901**, *2*, 559.

[51] L. Smith, A tutorial on principal components analysis, http://www.cs.otago.ac.nz/cosc453/student_tutorials/principal_components.pdf. Accessed: 2016-11-30, **2002**.

[52] I. Jolliffe, *Principal Component Analysis*, 2nd ed., Springer-Verlag, New York, USA **2002**.

[53] S. Han, B. Feeny. *J. Vib. Control* **2002**, *8*(1), 19.

[54] V. Lenaerts, G. Kerschen, J. Golinval. *J. Sound Vib.* **2003**, *262*(4), 907.
[55] G. Kerschen, B. Feeny, J. Golinval. *Comput. Methods Appl. Mech. Eng.* **2003**, *192*(13), 1785.
[56] P. De Boe, J. Golinval. *Struct. Health Monit.* **2003**, *2*(2), 137.
[57] D. García, I. Trendafilova. *J. Sound Vib.* **2014**, *333*(25), 7036.
[58] A. Yan, G. Kerschen, P. De Boe, J. Golinval. *Mech. Syst. Signal Process.* **2005**, *19*(4), 847.
[59] A. Yan, G. Kerschen, P. De Boe, J. Golinval. *Mech. Syst. Signal Process.* **2005**, *19*(4), 865.
[60] E. Reynders, G. Wursten, G. De Roeck. *Struct. Health Monit.* **2013**, *13*(1), 82.
[61] V. Nguyen, J. Mahowald, S. Maas, J. Golinval. *Shock Vib.* **2014**, *2014*, Article ID 872492.
[62] S. Hoell, P. Omenzetter. *J. Phys. Conf. Ser.* **2015**, *628*(1), Article ID 012068.
[63] D. Tibaduiza, L. Mujica, J. Rodellar. *Struct. Control Health Monit.* **2013**, *20*(10), 1303.
[64] M. Li, T. L. Huang, W. X. Ren. *Zhendong yu Chongji/J. Vib. Shock* **2011**, *30*(5), 83.
[65] K. Koo, J. Lee, C. B. Yun, in *Proceedings of the 17th ICAC World Congress*, *17*, Seoul, South Korea **2008**, *17*(2), 15762.
[66] H. Li, S. Li, J. Ou, H. Li. *Struct. Control Health Monit.* **2010**, *17*(5), 495.
[67] S.-S. Jin, S. Cho, H.-J. Jung. *Comput. Struct.* **2015**, *158*, 211.
[68] A. Bellino, A. Fasana, L. Garibaldi, S. Marchesiello. *Mech. Syst. Signal Process.* **2010**, *24*(7), 2250.
[69] K. Roy, S. Ray-Chaudhuri. *J. Sound Vib.* **2013**, *332*(21), 5584.
[70] N. Navabian, M. Bozorgnasab, R. Taghipour, O. Yazdanpanah. *Arch. Appl. Mech.* **2016**, *86*(5), 819.
[71] Y. Bai, S. He, W. Nie, J. Gao, X. Song, in *Proceedings of the 1st International Conference on Advances in Computational Modeling and Simulation 2011, ACMS 2011*, vol. *31*, Kunming, China, **2012**, 534.
[72] F. Grubbs. *Technometrics* **1969**, *11*(1), 1.

How to cite this article: Shokrani Y, Dertimanis VK, Chatzi EN, Savoia MN. On the use of mode shape curvatures for damage localization under varying environmental conditions. *Struct Control Health Monit*. 2018;25:e2132. https://doi.org/10.1002/stc.2132

APPENDIX A: THE GRUBBS' TEST

The Grubbs' test[72] aims at detecting a single outlier from a sample $\mathbf{x} = [x_1, x_2, \dots, x_N]$ of univariate data that follows approximately the normal distribution. This is succeeded through the hypothesis test,

H0: The data set contains no outliers.
H1: The data set contains exactly one outlier.

which is treated at a significant level α. The current study implements the two-sided version of the test, in which the Grubbs' statistic is defined as

$$G = \frac{\max\{|\mathbf{x} - \mu_x|\}}{\sigma_x},$$

where μ_x and σ_x are the mean and the standard deviation of the sample, respectively. The critical Grubbs' value reads

$$G_{cr} = \frac{N-1}{\sqrt{N}} \sqrt{\frac{\left(t_{\frac{\alpha}{2N},N-2}\right)^2}{N-2+\left(t_{\frac{\alpha}{2N},N-2}\right)^2}}$$

with $t_{\frac{\alpha}{2N},N-2}$ denoting the critical value of the t-distribution at a $\alpha/(2N)$ significance level and $N-2$ degrees of freedom. The null hypothesis (H0) is rejected if $G > G_{cr}$.